

Cite this: *J. Mater. Chem. A*, 2017, 5, 9272

Rapid exfoliation of layered covalent triazine-based frameworks into N-doped quantum dots for the selective detection of Hg²⁺ ions†

Yuanzhi Zhu,^{‡a} Man Qiao,^{‡b} Wenchao Peng,^a Yang Li,^a Guoliang Zhang,^a Fengbao Zhang,^a Yafei Li^{*b} and Xiaobin Fan^{ID *a}

Metal-free carbon quantum dots (CQDs) have attracted great interest, but the rapid preparation of doped CQDs with tunable optical properties is still an urgent task. Herein, we report that covalent organic frameworks (covalent triazine-based frameworks, CTF-1) with layered structures can be rapidly exfoliated and cut into N-doped CQDs. The cutting mechanism involves triazine hydrolysis and breaking the bonds between the triazines and benzene rings. Experiments and density functional theory (DFT) calculations confirm that the fluorescence of the obtained CQDs mainly originates from the intrinsic state emission induced by localized $\pi-\pi^*$ transitions, despite the contribution of the defect state emission. Due to their unique chemical structure, the CQDs could be further utilized as an efficient PL probe for detecting Hg²⁺. This study may open up new avenues for developing new kinds of CQDs using covalent organic frameworks as the starting materials.

Received 15th February 2017
Accepted 31st March 2017

DOI: 10.1039/c7ta01438d

rsc.li/materials-a

Introduction

Inorganic quantum dots (QDs) have attracted great research interest for their tunable emission, broad excitation bands, and resistance against photobleaching compared to traditional organic dyes.^{1,2} Nevertheless, normal inorganic QDs still suffer from serious health and environmental concerns because of their metal composition.³ As a new generation of luminescent materials, metal-free carbon quantum dots (CQDs) have been proven to be promising alternatives for QDs in applications that are sensitive to metal contamination, such as biosensors, bio-imaging, metal ion detection, *etc.*⁴⁻⁸ Compared to common QDs, the most striking properties of CQDs are their good dispersibility, low toxicity, biocompatibility and high chemical stability.⁹ Moreover, their physicochemical properties can be further tuned through heteroatom doping.¹⁰ For instance, doping CQDs with N heteroatoms could effectively modulate their band gap to make them promising candidates for photocatalysis.^{11,12} Nitrogen-doping can also improve the sensitivity

and selectivity of CQDs for the fluorescence detection of metal ions.¹³ Controlling the doping of N could passivate the surface states of CQDs and realize the transformation from excitation-dependent emission to excitation-independent emission.¹⁴ Other dopants such as the S atom were also found to possess a cooperative effect with the N atom in enhancing the quantum yield (QY) of CQDs.¹⁵

In contrast to the bottom-up strategy that can obtain doped CQDs by using heteroatom-containing precursors, top-down methods from bulk crystals for the preparation of doped CQDs are seldom reported, despite their potential low cost and simple operation.^{16,17} This might be hampered by the lack of suitable carbon starting materials with desired heteroatoms. Recently, graphitic carbon nitride has been successfully broken down into N-doped CQDs for various applications.¹⁸⁻²⁰ However, exploring new candidates and developing more efficient methods to synthesize doped CQDs on a large scale are still urgent tasks.

Covalent organic frameworks (COFs) are a new type of porous polymer with pure organic nanostructures, extended π -conjugation and well-defined crystallinity.²¹⁻²³ Their chemical components and optical properties can be tailored by selectively choosing various organic molecules as the building blocks.²⁴⁻²⁶ Therefore, we proposed that COFs may be used as ideal candidates for the top-down preparation of doped CQDs. To test this idea, we herein report the successful exfoliation and cutting of the low-cost layered covalent triazine-based frameworks (CTF-1)^{27,28} into N-doped quantum dots (CTFQDs). The detailed mechanisms involved and the origin of the luminescence were systematically investigated. The obtained CTFQDs were also

^aSchool of Chemical Engineering and Technology, State Key Laboratory of Chemical Engineering, Collaborative Innovation Center of Chemical Science and Engineering, Tianjin University, Tianjin, 300072, China. E-mail: liyafei@njnu.edu.cn

^bSchool of Chemistry and Materials Science, Jiangsu Key Laboratory of New Power Batteries, Jiangsu Collaborative Innovation Centre of Biomedical Functional Materials, Nanjing Normal University, Nanjing, 210023, China. E-mail: xiaobinfan@tju.edu.cn

† Electronic supplementary information (ESI) available: Additional experimental results (S1–S8) and detailed computational methods (PDF). See DOI: 10.1039/c7ta01438d

‡ The authors contributed equally to the work.

utilized as a photoluminescence probe for the rapid, sensitive and selective detection of Hg^{2+} ions.

Experimental

Synthesis of layered covalent triazine-based frameworks (CTF-1) or amorphous covalent triazine-based frameworks (A-CTF)

The samples were synthesized according to the literature.²⁷ In brief, the 1,4-dicyanobenzene monomer (1 g) and ZnCl_2 (1.06 g for CTF-1 and 5.3 g for A-CTF) were transferred into a glass ampoule (2 cm \times 15 cm) under an inert atmosphere. The ampoule was evacuated, sealed, heated (5 $^\circ\text{C min}^{-1}$) and kept at a terminal temperature of 400 $^\circ\text{C}$ for 40 h. The ampoule was then cooled down to room temperature and opened. The resulting powder was finely ground and washed with 0.1 M HCl, water, acetone and chloroform. Finally, the powder was vacuum dried overnight at 60 $^\circ\text{C}$.

Synthesis of the CTFQDs

500 mg of the CTF-1 or A-CTF powder was dispersed in 20 mL of concentrated sulfuric acid (98%) and stirred at room temperature for 6 hours. The mixed solution was heated to the desired temperature (100 $^\circ\text{C}$, 130 $^\circ\text{C}$ or 160 $^\circ\text{C}$) and then 6 mL of H_2O_2 (30% in water) was dropped into the solution slowly. The CTF-1 or A-CTF powders were rapidly dissolved with large amounts of bubbles. The wine-red or yellow solution was obtained within 5 minutes. Further raising of the initial temperature to over 160 $^\circ\text{C}$ hardly improved the cutting efficiency, probably because of the fast degradation of H_2O_2 at higher temperatures.

Caution: The reaction must be processed in an unsealed reactor because it can generate large amounts of O_2 . Addition of H_2O_2 into H_2SO_4 inevitably leads to heat release. Hence, the addition of H_2O_2 should be slow enough to reduce the increase in temperature as much as possible.

Purification of the CTFQDs

The obtained CTFQDs in H_2SO_4 solution were diluted with deionized water (250 mL) and filtered through a 0.22 μm PTFE membrane to remove the unreacted CTF-1. Unreacted H_2SO_4 was neutralized with NaOH to generate Na_2SO_4 . 500 mL of methanol was slowly dropped into the solution to conduct the antisolvent crystallization of Na_2SO_4 . The precipitated Na_2SO_4 and methanol were removed by filtration and a rotary evaporator at 70 $^\circ\text{C}$. The same antisolvent crystallization process was performed again using ethanol (300 mL) as the antisolvent. The obtained CTFQD aqueous solution can be further dialyzed in a dialysis bag (retained molecular weight: 500–1000 Da) overnight. The CTFQD powder was obtained by freeze-drying.

Detection of Hg^{2+} ions

1 mL of CTFQD-160 aqueous solution (70 $\mu\text{g mL}^{-1}$) was added to a quartz cuvette, followed by the addition of different concentrations of a Hg^{2+} ion aqueous solution and equilibration for 1 min before the spectral measurements were taken. The selectivity for Hg^{2+} ions was confirmed by adding other metal ion aqueous solutions instead of Hg^{2+} ions in a similar

way. The fluorescence spectra were recorded under excitation at 290 nm.

Characterization

Samples were characterized by X-ray diffraction (Bruker D8 FOCUS, Cu-K α radiation), Raman spectroscopy (NT-MDT with 433 nm laser excitation), X-ray photoelectron spectroscopy (PHI5000 Versa Probe), ^{13}C solid-state nuclear magnetic resonance spectroscopy (BRUKER AvanceIII HD 500 MHz), Fourier transform infrared spectroscopy (Bruker VERTEX 80), transmission electron microscopy (JEM-2100F), atomic force microscopy (CSPM5500, BENYUAN), UV-vis spectroscopy (3802 UNIC, Beijing), fluorescence spectrophotometry (Hitachi F2500) and X-ray fluorescence spectroscopy (S4 Pioneer). The absolute quantum yields of the CTFQDs solutions were determined using the FLS980 series of fluorescence spectrometers. All samples were diluted with DI water to avoid reabsorption.

Results and discussion

The successful synthesis of layered CTF-1 through the polymerization of dicyanobenzene in molten ZnCl_2 was confirmed by X-ray diffraction (XRD) and Raman measurements (Fig. S1 and S2, ESI †).²⁷ Because the CTF-1 is highly chemically stable, a strongly oxidizing piranha solution (mixture of H_2SO_4 and H_2O_2) was used for the intercalation and cutting of the CTF-1 skeleton at different temperatures (Fig. 1a). We found that the CTF-1 could be successfully exfoliated when the H_2O_2 (34% in water) was added dropwise into the CTF-1/ H_2SO_4 solution at an elevated temperature (*e.g.* 160 $^\circ\text{C}$) and a wine-red to yellow dispersion could form rapidly within 5 minutes (Fig. 1b). Unreacted sulphuric acid could be easily removed by neutralization and antisolvent crystallization with methanol (see details in the Experimental section). After rotary evaporation and freeze-drying, the off-white fluffy CTFQD powder was obtained with a yield of $\sim 45\%$ (Fig. 1c).

Subsequent careful characterization by X-ray photoelectron spectroscopy (XPS) revealed that the cutting mechanism mainly involves triazine hydrolysis and breaking the bonds between the triazines and benzene rings. The high-resolution C1s spectra of the obtained CTFQDs (Fig. 2a) show the co-existence of abundant aromatic rings (284.6 eV) and the C=N bonds (286.4 eV) in the triazine rings, suggesting that the CTFQDs maintain the same backbone as the pristine CTF-1. Meanwhile, a new peak at 285.6 eV is observed for the CTFQDs, which can be explained by the formation of C-OH at the edges of the CTFQDs during triazine hydrolysis.²⁹ Besides, the small peak (288.6 eV) assigned to -COOH slightly increased, because of the unreacted cyano group (-C \equiv N) in the CTF-1 skeleton or the -OH group can be converted into a carboxyl group under strongly acidic conditions.³⁰ According to the literature, triazine hydrolysis under acidic conditions not only results in cyanuric acid-like derivatives,^{18,31} but also generates amidine-like derivatives through ring open reactions.^{32,33} These assumptions were also testified by high-resolution N1s spectra (Fig. 2b). Consistent with previous studies, the N1s spectra of the CTF-1 can be

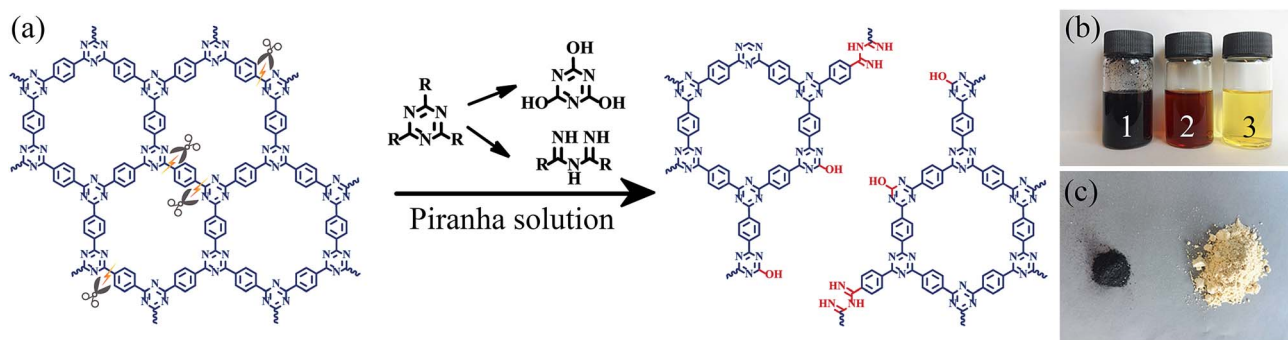


Fig. 1 (a) A possible mechanism for the exfoliation of the CTF-1 in piranha solution. (b) Digital photo of the CTF-1 in sulfuric acid (1), the obtained CTFQD dispersion (2) and the CTFQD dispersion after being diluted (3). (c) Digital photo of 500 mg of the CTF-1 powder (left) and the obtained CTFQD powder (right). The reaction was carried out at 160 °C.

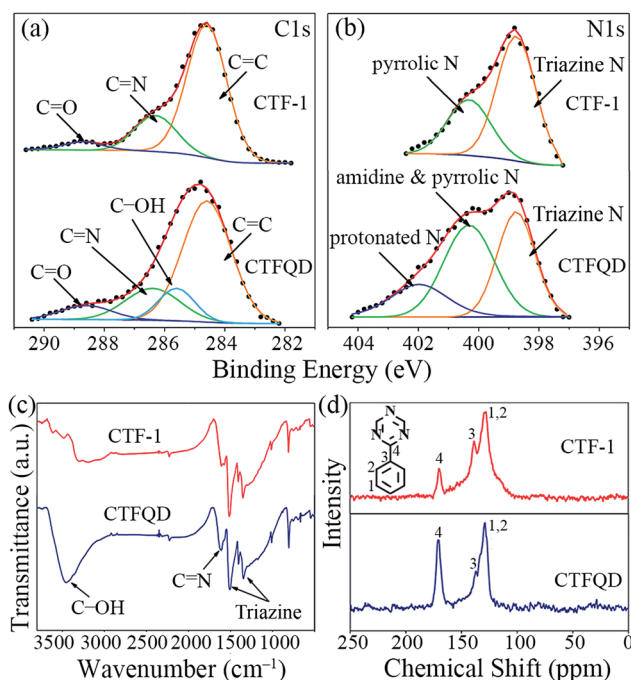


Fig. 2 (a) C1s X-ray photoelectron spectroscopy (XPS) of the pristine CTF-1 and the obtained CTFQDs. (b) The N1s XPS of the CTF-1 and the CTFQDs. (c) The FT-IR spectra of the CTF-1 and the CTFQDs. (d) Solid-state ^{13}C NMR of the CTF-1 and the CTFQDs. The CTFQDs were prepared at 160 °C.

deconvoluted into two main peaks with binding energies of 398.8 and 400.3 eV, corresponding to the triazine units in the CTF-1 and the pyrrolic-like nitrogen atoms (C–N–C) derived from triazine decomposition respectively.³⁴ After reaction with piranha solution, the triazine peak decreased, in accordance with the increase in the decomposition-derived nitrogen peak and the presence of the proton C=NH²⁺ (or NH³⁺) peak. These results indicate the presence of ring open reactions in the CTF-1 during treatment with piranha solution.

Similar results were also observed by Fourier transform infrared (FTIR) spectroscopy as shown in Fig. 2c. Compared to the pristine CTF-1, the obtained CTFQDs show new peaks which

were assigned to a –OH stretching vibration at 3458 cm⁻¹ and a stronger stretching vibration of non-conjugate C=N at 1610 cm⁻¹. Notably, the ^{13}C NMR spectra show a decrease in the resonance peaks of the benzene rings (129 ppm), and the C–C bonds between the benzene and triazine rings (137 ppm) become much less prominent.³⁴ Consistent with the ^{13}C NMR results, the ratio of C=C to C=N (estimated by the peaks' areas in the corresponding XPS spectra) decreases from 3.55 for the CTF-1 to 3.42 for the obtained CTFQDs. All of these results mean that the chemical tailoring mainly occurs at the C–C bonds between the benzene and triazine rings, leading to a loss of the benzene components.

Morphology characterizations by transmission electron microscopy (TEM) and atomic-force microscopy (AFM) confirmed that the CTF-1 was exfoliated and cut into nanosheets with lateral sizes that could be controlled by reaction temperature. For example, representative TEM images show that the nanosheets synthesized at 160 °C (CTFQD-160) have circular shapes and an average diameter of ~25 nm, ranging from 15 to 35 nm (Fig. 3a). The sizes of the nanosheets with irregular edges significantly increased when the reactions were carried out at lower temperatures, as illustrated in Fig. 3c (CTFQD-130, synthesized at 130 °C) and Fig. 3e (CTFQD-100, synthesized at 100 °C). Interestingly, the apparent heights of all the samples measured by AFM are in the range of 0.7 to 3 nm (Fig. 3b, d and f). As a typical 2D material, graphene always shows a larger AFM apparent thickness (~0.7 nm) than the theoretical value (~0.34 nm), which is attributed to the intrinsic out-of-plane deformation, as well as the instrumental offset arising from different interaction forces between the AFM probe, graphene, and the substrate.³⁵ Considering the fact that the CTF-1 has the same theoretical thickness as graphene,²⁷ the layer number of most of the obtained CTFQDs should be in the range of 1 to 4 layers, which is attributed to the simultaneous exfoliation and cutting of the layered CTF-1.

The UV-vis spectra of the CTFQDs show size-dependent properties (Fig. 4). One main peak at ~236 nm comes from the π - π^* electronic transitions in the CTF-1 skeleton containing triazine rings.^{18,20} It shows a prominent increase with decreasing CTFQDs size, which can be explained by the

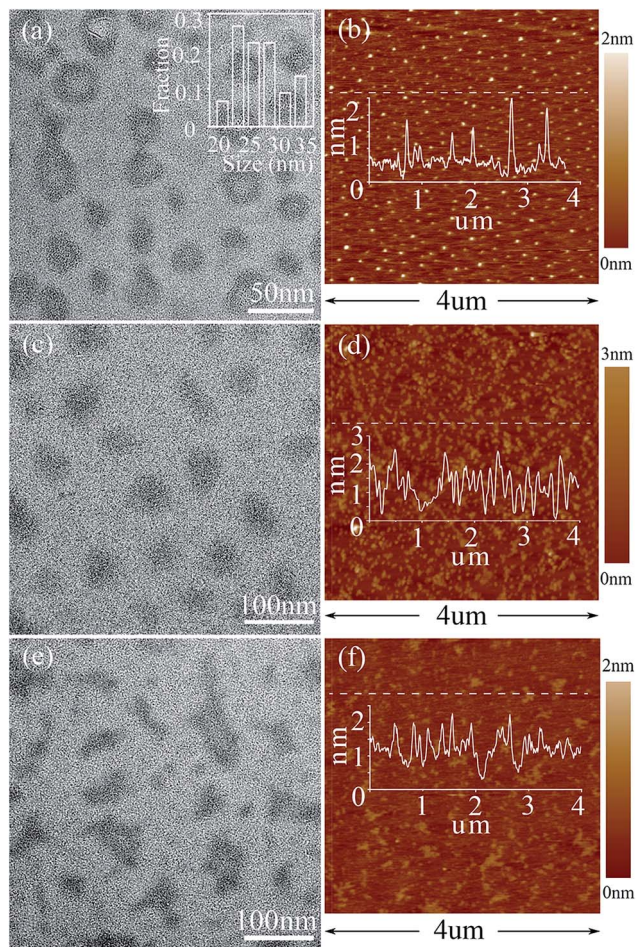


Fig. 3 (a) and (b) are the TEM and AFM results of CTFQD-160. (c) and (d) are the TEM and AFM results of CTFQD-130. (e) and (f) are the TEM and AFM results of CTFQD-100.

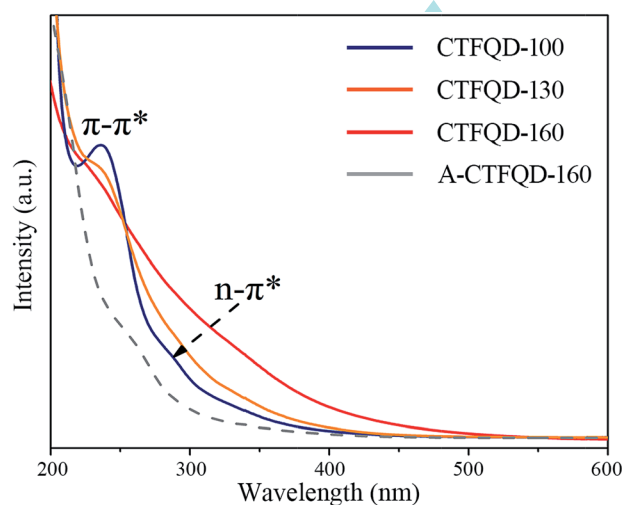


Fig. 4 The UV-vis spectra of the CTFQDs synthesized at 160 °C, 130 °C and 100 °C and the amorphous A-CTFQD (synthesized at 160 °C).

quantum confinement effect.³⁶ Another shoulder peak around 288 nm was assigned to the $n-\pi^*$ transition of the C=O or C=N and also became obvious when the sizes decreased,^{15,37} because the smaller sized CTFQDs should have more functional groups at the edge or more defects. To further probe the origin of these two peaks, an amorphous covalent triazine-based framework was used to synthesize the amorphous counterpart (labeled as A-CTFQD) under the identical synthesis conditions of CTFQD-160. As expected, only one shoulder peak corresponds to the $n-\pi^*$ transition that can be found in the UV-vis spectrum of the A-CTFQD (gray dash line in Fig. 4), while the $\pi-\pi^*$ peak is completely absent due to a lack of extended π -conjugation.

First-principle density functional theory (DFT) calculations of single-layered CTF-1 show a main absorption peak located at 310 nm in the calculated optical absorption spectra (Fig. 5a). The density of states (DOS) analysis (Fig. 5b) revealed that the transition energy of this peak (3.99 eV) agrees well with the HOMO-LUMO gap (3.94 eV). Specifically, the HOMO consists of π -type bonds in benzene-like C_6H_4 rings and lone pairs of N atoms, while the LUMO mainly originates from the π^* orbitals of C_3N_3 rings (Fig. 5c and d). According to the partial DOS, the HOMO of CTF-1 mainly consists of the $2p_z$ states of C atoms and with partial contribution from the $2p_z$ states of the N atoms, whereas the LUMO comprises equal contributions of the $2p_z$ states of the C and N atoms. The above results imply that both the HOMO and LUMO exhibit π -type bonding character. Importantly, the experimentally detected main absorption peak in the UV region should correspond to the $\pi-\pi^*$ transition, despite the obvious discrepancy in position that is probably caused by the size effects.²⁰

The PL spectra show that the emission maxima (excited at 290 nm) are blue-shifted from 460 nm for CTFQD-100 to 390 nm for CTFQD-160 (Fig. 6a). In addition, the PL intensities follow the trend of CTFQD-160 > CTFQD-130 > CTFQD-100, and the A-

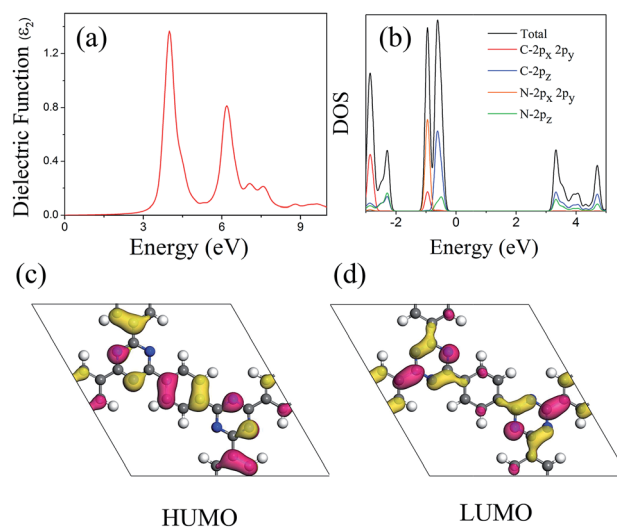


Fig. 5 (a) The imaginary part of the dielectric function of CTF-1. (b) Density of states of CTF-1. (c) and (d) show the partial charge densities associated with the HOMO and LUMO, respectively.

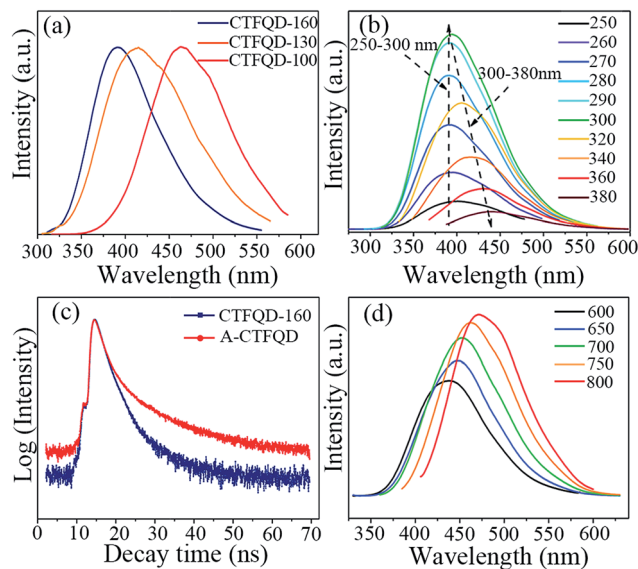


Fig. 6 (a) The PL spectra of the CTFQDs synthesized at 160 °C, 130 °C and 100 °C. (b) The PL spectra of CTFQD-160 with varying excitation wavelengths. (c) The fluorescence decay curves for CTFQD-160 and A-CTFQD. (d) The up-conversion PL property for CTFQD-160.

CTFQDs emit much weaker blue fluorescence than the CTFQD-160 at emission maxima of ~ 400 nm (Fig. S3[†]). Notably, this result is consistent with the increasing trend of the $\pi-\pi^*$ peak in the UV-visible spectrum. Therefore, we believe that the intrinsic state emission induced by a localized $\pi-\pi^*$ transition should play a critical role in the fluorescence. Previous studies suggested that the fluorescence of graphene or G-C₃N₄ based quantum dots can arise from the intrinsic state emission or the defect state emission which involves the presence of carbonyl- or amine-related groups.^{37–44} Therefore, the functional groups at the edge may also contribute to the fluorescence.

To confirm this hypothesis, the optical properties of the highly photoluminescent CTFQD-160 were systematically investigated. Fig. 6b shows the PL spectra for CTFQD-160 at various excitation wavelengths. The emission is excitation-independent when the excitation wavelength is below 300 nm, exceeding which an obvious red-shift occurred. The normalized PL excitation (PLE) spectra recorded at detection emission wavelengths (λ_{de}) from 360 nm to 480 nm are shown in Fig. S4.[†] The maximum PLE intensity was found to remain constant at ~ 285 nm, but the absorption tail gradually broadens with increasing λ_{de} . Such PL behavior is similar to previous reports on graphene oxide or graphene oxide quantum dots, which show the coexistence of intrinsic state emission and defect state emission.^{36,38,41,44,45} Time resolved PL spectra were performed to study the recombination dynamics of CTFQD-160 and A-CTFQD (Fig. 6c). Both samples show a bi-exponential decay curve with fast and slow decay components, corresponding to recombination from the intrinsic states and the defect states, respectively.^{42,45} The fast decay component dominates the emission from CTFQD-160, whereas the slow decay component increases substantially in A-CTFQD. All of these results support the conclusion that the PL mechanism of CTFQDs mainly relies on

the intrinsic state, but the functional groups also have some contribution. The pH-dependent PL behavior also supports our proposed PL mechanism. The PL emission of CTFQD-160 becomes stronger when the pH changes from 3 to 10 (Fig. S5[†]). This is because more N was protonated at lower pH, thus leading to the deactivation of the emissive state.

We found that the absolute fluorescence quantum yield (QY) of the CTFQDs can be efficiently improved by simple hydrothermal treatment without any additives. After an unoptimized process at 180 °C for 10 h, the QY of CTFQD-160 increased from 6.83% to 12.53%. The TEM analysis shows no obvious change in size after hydrothermal treatment (Fig. S6[†]). The UV-visible spectrum shows that the oxidation-induced shoulder peak is weaker (Fig. S7[†]). The maximum PL emission position did not change but the absorption tail decreased slightly compared to before (Fig. S8[†]). The C1s XPS analysis revealed a reduction in the C–OH component (Fig. S9[†]). Based on these observations, we believe that the reduction of oxygen functional groups can decrease the emissive traps induced by the defect states of functional groups, thus can suppress the non-radiative process and further enhance the intrinsic state emission.⁴⁴

The CTFQD-160 was found to exhibit obvious up-conversion properties (Fig. 6d). The up-conversion PL behavior of CTFQD-160 is similar to its down-conversion excitation-dependent PL behavior. The emission wavelength redshifts and PL intensity increases when changing the excitation wavelength from 600 to 800 nm. Interestingly, the A-CTFQD does not show similar up-conversion PL behavior. At present, the up-conversion PL behavior has not been clearly studied; it is generally attributed to a two or multiphoton active process.^{6,19,41} Our findings suggest that the extended π -conjugation may play an important role in the up-conversion PL behavior.

To explore the applications of the CTFQDs, photoluminescence detection of mercury ions (Hg²⁺) was investigated. Hg²⁺ is widely found in aquatic systems and can seriously threaten human health even at very low concentrations, due to its strong toxicity and bioaccumulation. Therefore, sensitive and quantitative determination of Hg²⁺ is of great importance. Fig. 7a shows the PL spectra of a CTFQD-160 solution in the presence of different concentrations of Hg²⁺ ions. The fluorescence of CTFQD-160 can be effectively quenched by Hg²⁺ ions within two minutes, and the colour change can be clearly recognizable by the naked eye. The Fig. 7b insert presents a graph of the PL intensity *versus* the concentration of Hg²⁺ ions. A good linear correlation ($R^2 = 0.997$) is shown in the concentration range between 0 and 30 μM . The limit of detection (LOD) was estimated to be 0.23 μM based on three times the standard deviation rule ($\text{LOD} = 3S_d/\text{slope}$), compared to the efficient Hg²⁺ fluorescent probe that has been previously reported.^{46,47} In general, Hg²⁺ ions have a tendency to coordinate with nitrogen atoms due to their unshared electrons. It is believed that the triazine units and the edge nitrogenous group of the CTFQDs can efficiently coordinate with Hg²⁺, deactivating the PL emission state to cause fluorescence quenching. Fig. 7b shows the percentage PL quenching of the CTFQDs in the presence of different metal ions. It was found that the CTFQDs exhibit

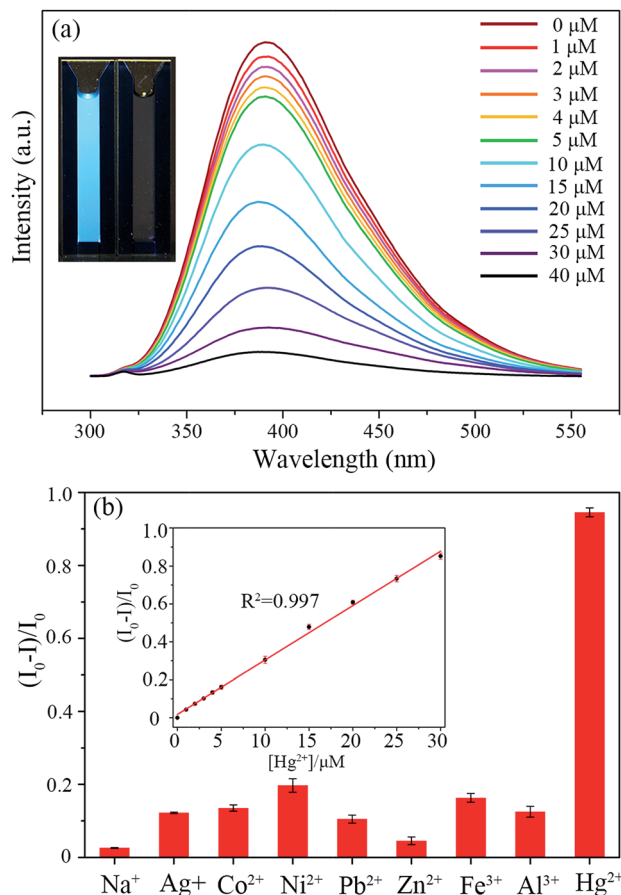


Fig. 7 (a) Fluorescence emission spectra of CTFQD-160 in aqueous solution upon addition of various concentrations of Hg^{2+} under excitation at 290 nm. Inset: digital photo showing the fluorescence emission change (under UV lamp with 365 nm center wavelength) of CTFQD-160 upon the addition of Hg^{2+} . (b) Selective PL response of CTFQD-160 aqueous solution for 40 μM of various metal ions. The inset shows the linear relationship between the PL intensity and Hg^{2+} concentration. The error bars represent the standard deviation of three independent measurements.

excellent selectivity for Hg^{2+} over other metal ions, probably due to its strongest coordination ability.

Conclusions

In summary, in this contribution we have demonstrated that the CTF-1 can be rapidly exfoliated and cut into N-doped CTFQDs in piranha solution. The cutting mechanism may involve triazine hydrolysis and breaking the bonds between the triazine and benzene rings. The control sample comes from the amorphous counterpart of CTF-1 and was used to aid the understanding of the fluorescence origin of the CTFQDs. As a result, the intrinsic state emission induced by localized π - π^* transitions plays the leading role in the CTFQDs and the defect state also contributes to the fluorescence. The QY of the CTFQDs can be effectively enhanced through hydrothermal treatment, probably because of the suppression of the non-radiative process and the enhancement in intrinsic state

emission. Due to its unique chemical structure, the CTFQDs could be further utilized as an efficient PL probe for detecting Hg^{2+} . Our proposed methodology may open up new avenues for developing new kinds of CQDs using COFs as the starting materials.

Acknowledgements

This study is supported by the National Natural Science Funds (No. 21676198; No. 21403115) and the Program of Introducing Talents of Discipline to Universities (No. B06006).

Notes and references

- U. Resch-Genger, M. Grabolle, S. Cavaliere-Jaricot, R. Nitschke and T. Nann, *Nat. Methods*, 2008, **5**, 763–775.
- I. L. Medintz, H. T. Uyeda, E. R. Goldman and H. Mattoussi, *Nat. Mater.*, 2005, **4**, 435–446.
- J. Shen, Y. Zhu, X. Yang and C. Li, *Chem. Commun.*, 2012, **48**, 3686–3699.
- S. Y. Lim, W. Shen and Z. Gao, *Chem. Soc. Rev.*, 2015, **44**, 362–381.
- Y. P. Sun, B. Zhou, Y. Lin, W. Wang, K. A. Fernando, P. Pathak, M. J. Mezziani, B. A. Harruff, X. Wang, H. Wang, P. G. Luo, H. Yang, M. E. Kose, B. Chen, L. M. Veca and S. Y. Xie, *J. Am. Chem. Soc.*, 2006, **128**, 7756–7757.
- G. Yang, X. Wan, Y. Su, X. Zeng and J. Tang, *J. Mater. Chem. A*, 2016, **4**, 12841–12849.
- H. K. Sadhanala, R. Nandan and K. K. Nanda, *J. Mater. Chem. A*, 2016, **4**, 8860–8865.
- L. Xu, G. Fang, J. Liu, M. Pan, R. Wang and S. Wang, *J. Mater. Chem. A*, 2016, **4**, 15880–15887.
- H. Li, Z. Kang, Y. Liu and S.-T. Lee, *J. Mater. Chem.*, 2012, **22**, 24230.
- Y. Park, J. Yoo, B. Lim, W. Kwon and S. W. Rhee, *J. Mater. Chem. A*, 2016, **4**, 11582–11603.
- L.-C. Chen, C.-Y. Teng, C.-Y. Lin, H.-Y. Chang, S.-J. Chen and H. Teng, *Adv. Energy Mater.*, 2016, **6**, 1600719–1600719.
- T. F. Yeh, C. Y. Teng, S. J. Chen and H. Teng, *Adv. Mater.*, 2014, **26**, 3297–3303.
- J. Ju and W. Chen, *Biosens. Bioelectron.*, 2014, **58**, 219–225.
- Y. H. Yuan, Z. X. Liu, R. S. Li, H. Y. Zou, M. Lin, H. Liu and C. Z. Huang, *Nanoscale*, 2016, **8**, 6770–6776.
- H. Ding, J. S. Wei and H. M. Xiong, *Nanoscale*, 2014, **6**, 13817–13823.
- Y. Du and S. Guo, *Nanoscale*, 2016, **8**, 2532–2543.
- D. Sun, R. Ban, P.-H. Zhang, G.-H. Wu, J.-R. Zhang and J.-J. Zhu, *Carbon*, 2013, **64**, 424–434.
- Z. Zhou, Y. Shen, Y. Li, A. Liu, S. Liu and Y. Zhang, *ACS Nano*, 2015, **9**, 12480–12487.
- X. Zhang, H. Wang, H. Wang, Q. Zhang, J. Xie, Y. Tian, J. Wang and Y. Xie, *Adv. Mater.*, 2014, **26**, 4438–4443.
- Z. Song, T. Lin, L. Lin, S. Lin, F. Fu, X. Wang and L. Guo, *Angew. Chem.*, 2016, **55**, 2773–2777.
- K. Sakaushi and M. Antonietti, *Acc. Chem. Res.*, 2015, **48**, 1591–1600.

- 22 J. Guo, Y. Xu, S. Jin, L. Chen, T. Kaji, Y. Honsho, M. A. Addicoat, J. Kim, A. Saeki, H. Ihee, S. Seki, S. Irle, M. Hiramoto, J. Gao and D. Jiang, *Nat. Commun.*, 2013, **4**, 2736.
- 23 X. Feng, X. Ding and D. Jiang, *Chem. Soc. Rev.*, 2012, **41**, 6010–6022.
- 24 G. Lin, H. Ding, D. Yuan, B. Wang and C. Wang, *J. Am. Chem. Soc.*, 2016, **138**, 3302–3305.
- 25 S. Y. Ding, M. Dong, Y. W. Wang, Y. T. Chen, H. Z. Wang, C. Y. Su and W. Wang, *J. Am. Chem. Soc.*, 2016, **138**, 3031–3037.
- 26 P. Kuhn, A. Thomas and M. Antonietti, *Macromolecules*, 2009, **42**, 319–326.
- 27 P. Kuhn, M. Antonietti and A. Thomas, *Angew. Chem.*, 2008, **47**, 3450–3453.
- 28 K. Sakaushi, E. Hosono, G. Nickerl, T. Gemming, H. Zhou, S. Kaskel and J. Eckert, *Nat. Commun.*, 2013, **4**, 1485.
- 29 I.-Y. Jeon, H. M. Kim, D. H. Kweon, S.-M. Jung, J.-M. Seo, S.-H. Shin, I. T. Choi, Y. K. Eom, S. H. Kang, H. K. Kim, M. J. Ju and J.-B. Baek, *Nano Energy*, 2016, **30**, 867–876.
- 30 J. An, L. Bagnell, T. Cablewski, C. R. Strauss and R. W. Trainor, *J. Org. Chem.*, 1997, **62**, 2505–2511.
- 31 A. Sattler, Ph.D. Thesis, Ludwig Maximilian University of Munich, Germany, 2010.
- 32 T. Kajiwara and T. Ito, *Eur. J. Inorg. Chem.*, 2004, **2004**, 3084–3088.
- 33 M. M. Turnbull, M. Y. Wei and R. D. Willett, *J. Coord. Chem.*, 2006, **35**, 11–17.
- 34 K. Schwinghammer, S. Hug, M. B. Mesch, J. Senker and B. V. Lotsch, *Energy Environ. Sci.*, 2015, **8**, 3345–3353.
- 35 X. Fan, W. Peng, Y. Li, X. Li, S. Wang, G. Zhang and F. Zhang, *Adv. Mater.*, 2008, **20**, 4490–4493.
- 36 S. H. Song, M.-H. Jang, J. Chung, S. H. Jin, B. H. Kim, S.-H. Hur, S. Yoo, Y.-H. Cho and S. Jeon, *Adv. Opt. Mater.*, 2014, **2**, 1016–1023.
- 37 L. Tang, R. Ji, X. Cao, J. Lin, H. Jiang, X. Li, K. S. Teng, C. M. Luk, S. Zeng, J. Hao and S. P. Lau, *ACS Nano*, 2012, **6**, 5102–5110.
- 38 J. Shang, L. Ma, J. Li, W. Ai, T. Yu and G. G. Gurzadyan, *Sci. Rep.*, 2012, **2**, 792.
- 39 H. Tetsuka, R. Asahi, A. Nagoya, K. Okamoto, I. Tajima, R. Ohta and A. Okamoto, *Adv. Mater.*, 2012, **24**, 5333–5338.
- 40 S. Zhu, Y. Song, X. Zhao, J. Shao, J. Zhang and B. Yang, *Nano Res.*, 2015, **8**, 355–381.
- 41 S. Zhu, J. Zhang, S. Tang, C. Qiao, L. Wang, H. Wang, X. Liu, B. Li, Y. Li, W. Yu, X. Wang, H. Sun and B. Yang, *Adv. Funct. Mater.*, 2012, **22**, 4732–4740.
- 42 C. T. Chien, S. S. Li, W. J. Lai, Y. C. Yeh, H. A. Chen, I. S. Chen, L. C. Chen, K. H. Chen, T. Nemoto, S. Isoda, M. Chen, T. Fujita, G. Eda, H. Yamaguchi, M. Chhowalla and C. W. Chen, *Angew. Chem.*, 2012, **51**, 6662–6666.
- 43 G. Eda, Y. Y. Lin, C. Mattevi, H. Yamaguchi, H. A. Chen, I. S. Chen, C. W. Chen and M. Chhowalla, *Adv. Mater.*, 2010, **22**, 505–509.
- 44 H. Yoon, Y. H. Chang, S. H. Song, E. S. Lee, S. H. Jin, C. Park, J. Lee, B. H. Kim, H. J. Kang, Y. H. Kim and S. Jeon, *Adv. Mater.*, 2016, **28**, 5255–5261.
- 45 F. Liu, M. H. Jang, H. D. Ha, J. H. Kim, Y. H. Cho and T. S. Seo, *Adv. Mater.*, 2013, **25**, 3657–3662.
- 46 R. Zhang and W. Chen, *Biosens. Bioelectron.*, 2014, **55**, 83–90.
- 47 J. B. Essner, C. H. Laber, S. Ravula, L. Polo-Parada and G. A. Baker, *Green Chem.*, 2016, **18**, 243–250.